Chinese Chemical Letters 34 (2023) 107867

Contents lists available at ScienceDirect

Chinese Chemical Letters

journal homepage: www.elsevier.com/locate/cclet

Highly efficient and non-doped red conjugated polymer dot for photostable cell imaging

Mengqi Wu[a], Qidong Wei[a], Caihong Xian[a], Chunlei Dai[a], Xuehan He[b], Changfeng Wu[c], Guoming Sun[d,*], Lei Chen[a,*]

[a] School of Biomedical Engineering, Sun Yat-sen University, Shenzhen 518107, China
[b] Teaching and Experiment Centre, Sun Yat-sen University, Shenzhen 518107, China
[c] Department of Biomedical Engineering, Southern University of Science and Technology, Shenzhen 518055, China
[d] College of Chemistry and Environmental Science, Hebei University, Affiliated Hospital of Hebei University, Baoding 071002, China

ARTICLE INFO

Article history:
Received 20 June 2022
Revised 16 September 2022
Accepted 28 September 2022
Available online 1 October 2022

Keywords:
Conjugated polymer dot
Cell imaging
Naphthothiadiazole
Photostability
Non-doped

ABSTRACT

By introducing a naphthothiadiazole (NT) unit as the main building block, a non-doped and red emissive conjugated polymer poly(9,9-dihexylfluorene-*alt*-naphthothiadiazole) (PFNT) is readily obtained through a two-step synthesis. Since the NT unit has a large twist angle with its neighboring segment, the aggregation-induced quenching (AIQ) effect of PFNT can be effectively suppressed in the condensed state. As a result, the corresponding PFNT polymer dot (Pdot) exhibits a high fluorescence quantum yield of 53.2% with peak emission at 616 nm, which is one of the most efficient red Pdots known. PFNT Pdot shows good biocompatibility and can be employed for living cell fluorescent imaging with high brightness. It also can be used for specific subcellular organelle imaging through immunofluorescence labeling. Furthermore, the PFNT Pdot demonstrates much better photostability for long-time cell fluorescence imaging than commercial red dyes. The high performances of PFNT Pdot make it a promising fluorescent probe for practical bioapplications.

During the past decade, water dispersible and biocompatible conjugated polymer dots (Pdots) have emerged as a new generation fluorescent probe for biomedical applications [1–5]. Similar to inorganic semiconductor quantum dots (Qdots), Pdots exhibit much higher brightness (1∼2 orders) than small molecular fluorescent probes while having no potential biotoxic issue of heavy-metallic Cd/Te atom containing Qdots [6]. In addition, they can be easily functionalized before or after the nanoformulation process through chemical bonding or physical blending methods for specific applications [7]. Pdots with various emissions ranging from deep-blue to second near-infrared window have been widely developed for cell and tissue imaging, bioassays, or optical diagnosis and therapy (optical therapeutic agents and nanocarriers for drug delivery) [8–14].

Highly efficient blue, green and orange emissive Pdots with fluorescent quantum yield (ϕ_f) close to or above 30% have been obtained using non-doped polymers, like poly(9,9-dioctylfluorene) (PFO), poly(9,9-dioctylfluorene-*alt*-benzothiadiazole) (PFBT) and poly[2-methoxy-5-(2-ethylhexyloxy)-1,4-(1-cyanovinylene-1,4-phenylene)] (CN-PPV) [15–17]. However, red and near-infrared (NIR) Pdots based on homogenous polymers usually show quite low ϕ_f [18], mainly because of their intrinsically small ground-excited state energy gap ($\Delta E_{S_n\text{-}S_0}$) and increased aggregation-induced quenching (AIQ) effect in condensed Pdot state [19], both of which may lead to enhanced non-radiative decay of excitons [20,21]. Red/NIR chromophores with rigid and planar structures can overcome the small $\Delta E_{S_n\text{-}S_0}$ nature and realize high ϕ_f in a diluted state because the non-radiative decay arising from molecular rotation and vibration can be effectively suppressed. Unfortunately, they tend to be severely self-quenching due to π-π stacking in the condensed state [22]. Therefore, people have primarily focused on ways to alleviate the AIQ effect and design red/NIR Pdots with high ϕ_f.

One common method is incorporating red/NIR chromophores into a blue/green polymer backbone to form a binary or ternary host/dopant system [23]. However, only a small number of red/NIR dopants (usually ≤3 mol%) could be integrated into the blue/green polymer matrix due to the self-quenching issue at higher molarity, especially for those dyes with narrow-band emission feature such as BODIPY, cyanine, or squaraine derivatives [24,25]. The low

* Corresponding authors.
E-mail addresses: gsun@hbu.edu.cn (G. Sun), chenlei59@mail.sysu.edu.cn (L. Chen).

https://doi.org/10.1016/j.cclet.2022.107867
1001-8417/

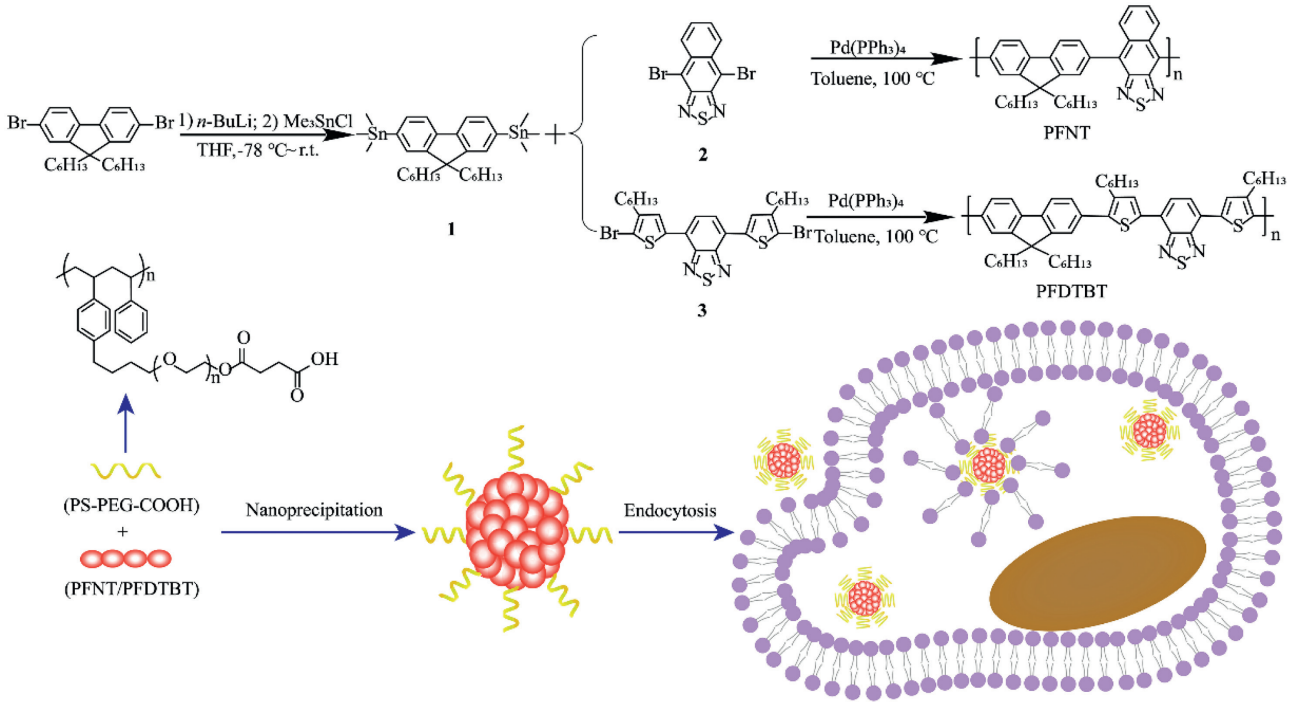

Scheme 1. Synthetic routes of PFNT and PFDTBT polymers and illustration of the corresponding PFNT Pdot for cellular imaging.

content of red/NIR emitters in polymer systems could cause diminished photostability of the resulting Pdots under stronger, longer-time laser excitation [26]. Besides, this type of Pdots only has intensive absorption in the short ultraviolet/blue wavelength region, which is unwanted for *in vivo* applications.

Efficient red/NIR Pdots based on non-doped polymers can be obtained by increasing the amphipathic surfactant to dilute the homogenous conjugated polymers in Pdots [27] but leading to a distinctly decreased extinction coefficient of the single nanoparticle. An alternative strategy is introducing highly twisted or aggregation-induced emission (AIE) moiety into the polymer backbone [22,28]. By replacing the 2,1,3-benzothiadiazole (BT) electron withdrawing segment of classic PFDTBT red polymer with 6,7-difluoro-2,3-bis(3-(hexyloxy)phenyl)quinoxaline unit, Chan group obtained a homogenous and deep-red emissive polymer PFTC6FQ [23]. The corresponding Pdot exhibits a relatively high ϕ_f of 47%, which is the most efficient red Pdot based on non-doped polymer as we know. After incorporating a small amount of BODIPY-based NIR emitter into the PFTC6FQ backbone, the resulting PFTC6FQ-BPDIPY NIR Pdot exhibits a ϕ_f of 33% [26]. Recently, by further alternating the planar 9,9-dioxylfluorene segment of the PFTFQ-BODIPY with an AIE-active tetraphenylethene (TPE) unit or torsional pentiptycene (PPTC) segment, the ϕ_f of resulting Pdots can be significantly improved from 7% of PFTFQ-BODIPY to 37% of TPETFQ-BODIPY and 51% of PTTCTFQ-BODIPY [29]. Living cell or *in vivo* tissue fluorescence imaging was successfully illustrated using these deep-red or NIR Pdots. Despite the ultrahigh ϕ_f, red/NIR polymers mentioned above have two drawbacks. Firstly, these polymers were obtained by complicated synthetic routes. Secondly, the introduced AIE moiety/twisted structure usually causes interrupted π-conjugation of the polymer backbone. This leads to pronounced blue-shifted absorption bands (~30 nm) compared to classic red PFDTBT Pdot, which is undesired for *in vivo* fluorescent imaging.

Herein, we report a non-doped poly(9,9-dihexylfluorene-*alt*-naphthothiadiazole) (PFNT) polymer as shown in Scheme 1. It can be easily synthesized from a commercially available monomer 4,9-dibromonaphthothiadiazole (NT-Br_2, intermediate **2**). The resulting PFNT Pdot shows a red emissive peak around 616 nm and a high ϕ_f up to 53.2%, among one of the most efficient red Pdots reported so far. Highly photostable living cell fluorescent imaging by confocal microscopy was achieved using the PFNT Pdot.

Table 1
The photophysical properties and size of polymers in THF and Pdot state.

Polymer	Status	λ_{abs} [a] (nm)	λ_{em} [a] (nm)	Φ_f [b] (%)	Size [c] (nm)
PFNT	THF	509	617	81.2	N.A.
	Pdot	509	616	53.2	28.1
PFDTBT	THF	507	627	75.8	N.A.
	Pdot	518	636	9.4	30.8

[a] Measured in diluted THF solution or Pdot aqueous with a concentration of 5 ppm.
[b] Absolute fluorescent quantum yield.
[c] Measured by DLS.

In this study, besides the ready availability, the NT unit was screened out as the building block for the following reasons. Firstly, it possesses a stronger electron-withdrawing ability due to one more benzene ring fused in its molecular structure than the benzothiadiazole (BT) unit. Due to enhanced molecular rigidity, its derivatives show red-shifted emission wavelengths with intrinsically high ϕ_f in single molecular status [30]. Secondly, the vertically extended phenyl ring of the NT core also leads to a larger twist angle with the neighboring segment [31], which can restrain the AIQ effect of its derivative emitters and remain high ϕ_f in the aggregated state [32,33]. Classic red polymer poly[(9,9-dihexyl-fluorene)-alt-(4,7-di-2-hexylthienyl-benzothiadiazole)] (PFDTBT) was also synthesized as a reference. The detailed synthesis and characterizations are shown in Supporting information.

The corresponding PFNT and PFDTBT Pdots were prepared by the nanoprecipitation method as previously described [34]. We encapsulated conjugated polymer using amphiphilic polystyrene with carboxylated polyethylene glycol (PS-PEG-COOH). The morphology and size of PFNT and PFDTBT nanoparticles were studied by transmission electron microscopy (TEM) and dynamic light scattering (DLS), as shown in Figs. 1A and B. As listed in Table 1, the number-

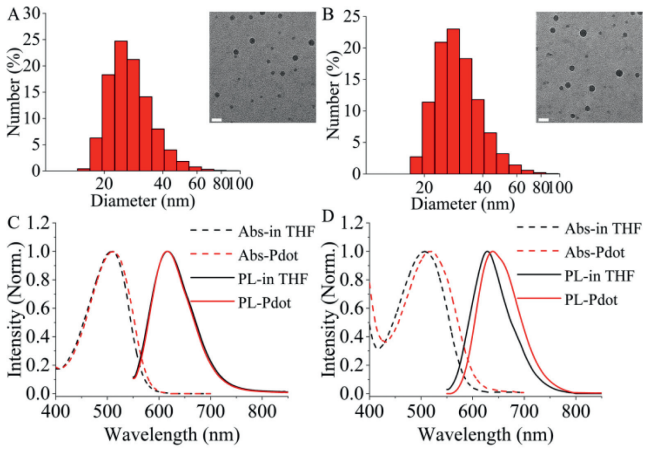

Fig. 1. The size distribution by DLS and TEM image for PFNT (A) and PFDTBT (B) Pdot (TEM scale bar: 50 nm). Abs and FL spectra of PFNT (C) and PFDTBT (D) in Pdot aqueous and THF solution.

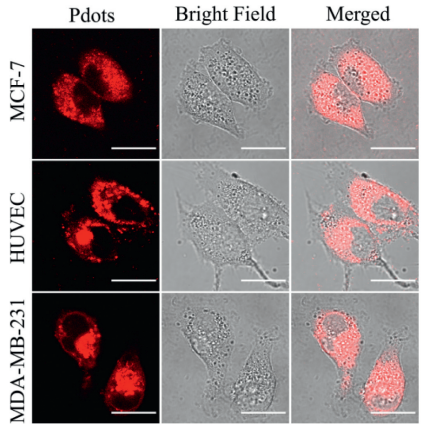

Fig. 2. Confocal fluorescence microscopy images of MCF-7, HUVEC, and MDA-MB-231 cells incubation with PFNT Pdot (Scale bar: 20 μm, λ_{ex}: 561 nm).

average hydrodynamics size of PFNT/PFDTBT Pdot measured by DLS was around 28 nm and 30 nm, respectively.

We further investigated the photophysical properties of PFNT and PFDTBT polymers in diluted THF solution and their Pdots aqueous. The absolute ϕ_f was measured by an integrated sphere, and the results are listed in Table 1. Both polymers possess relatively high ϕ_f in THF solution, 81.2% for PFNT and 75.8% for PFDTBT. The PFNT Pdot remains a high ϕ_f of 53.2%, while the PFDTBT Pdots show a sharply decreased ϕ_f of 9.4%. These results confirm the AIQ effect of PFNT polymer was dramatically lightened in the condensed Pdot state. It can be ascribed to the large dihedral degree of NT derivatives, inhibiting unwanted intermolecular interaction in the aggregation state. The alleviated intermolecular interaction of PFNT Pdot can be further verified by the absorption (Abs) and fluorescence (FL) spectra. As shown in Fig. 1C, PFNT illustrates almost the same Abs and FL spectra in THF solution and Pdot state, with absorption peaks at ~509 nm and an emission peak at 616 nm. In comparison, PFDTBT exhibits visibly red-shifted Abs and FL spectra in the Pdot state (Fig. 1D), suggesting an unavoidable AIQ effect. These optical properties indicate that introducing the NT unit to design PFNT polymer is a practical approach to reduce the AIQ effect and realize efficiently non-doped red emissive Pdot.

Next, we demonstrated the biological applicability of the non-doped PFNT Pdot. We first evaluated the cytotoxicity of PFNT Pdot towards MCF-7, HUVEC, and MDA-MB-231, three living cells, by MTT assay experiments. As shown in Fig. S1 (Supporting information), after 24 h of incubation with as high as 80 ppm PFNT Pdot, the cell viability has no significant decline. It demonstrates the excellent biocompatibility of PFNT Pdot, which is desirable for future biological applications. Then we performed fluorescence imaging on these three cells incubated with PFNT Pdot using confocal laser scanning microscopy (CLSM). Fig. 2 shows the apparent internalization of PFNT Pdot (20 ppm) after 24 h of incubation with the nanoparticles. Cells could uptake Pdot predominately into lysosome subcellular organelle *via* endocytosis (Fig. S2 in Supporting information), as studied in the previous report [35]. After internalization, the red emissive fluorescence with extraordinary brightness appears in the cytoplasm, excluding the nuclei, illustrating the different cell morphology of the three cells. Generally, the Pdot nanoprobes are well dispersed in cells with a few aggregates because Pdots may generate clusters in the physiological environment [36]. In addition, the bright-field images showed that cells were in good condition with no significant sign of apoptosis or inflammation, making PFNT Pdot a distinguished fluorescent probe for living cell imaging. Moreover, after bioconjugation with streptavidin (SA), PFNT Pdot-SA bioconjugates can label subcellular organelles, such as cell membranes and microtubules (Figs. S3 and S4 in Supporting information).

As mentioned above, one problem of dopant/host system-based Pdot probes is the declined photostability. It mainly originates from that part of the dopant emitters will be photobleached under strong and long-time laser excitation, along with an incomplete energy transfer from host to dopant. As a result, the photon budget from the dopant will decrease, and the host's fluorescence will increase. Theoretically, there should be no such problem for our non-doped PFNT Pdot. To investigate the photostability of PFNT Pdot, we performed the time-dependent dynamic confocal fluorescence images in labeled HUVEC cells, using two other commercial fluorescent dyes, Lyso-Tracker Red and CellTrace^{TM} Red CMTPX, as references. Because these two dyes share a staining pattern of lysosomes or cytoplasm labeling, similar to PFNT Pdot, their chemical structures are shown in Scheme S1 (Supporting information). HUVEC cells were stained with red dyes according to the instructions. After incubating these three red fluorescent probes without any anti-photobleaching reagent, we recorded the confocal fluorescence images of labeled HUVEC cells at 5 s intervals under the same irradiation conditions. Fig. 3 presents the superior photostability of the PFNT Pdot probe. The cell brightness labeled with commercial dyes decreased within 10 s and was almost completely quenched within 60 s. However, cells treated with PFNT Pdots show continuously stable fluorescence in 60 s as expected, with bare photobleaching. Furthermore, we used ImageJ software to evaluate the mean fluorescence intensity of the rectangle area at different time points (Fig. S5 in Supporting information). After the 13th irradiation, the brightness of PFNT, Lyso-Tracker Red, and CellTrace^{TM} Red CMTPX labeled cells are 94.0%, 25.1% and 8.9% of the initial value, respectively (Fig. 3D). These results reveal that the PFNT Pdot probe in cells owns much stronger photobleaching resistance than the reference dyes.

In summary, a non-doped and conjugated red polymer PFNT was easily obtained through a two-step synthesis by introducing a commercially available NT unit as the building block. Due to the significantly impeded AIQ effect, the corresponding PFNT Pdot exhibits an extraordinarily high ϕ_f of 53.2%, one of the most efficient red Pdots reported so far. It has low cytotoxicity verified by MTT assays. And *in vitro* fluorescent imaging of a series of living cells was demonstrated by simply endocytosing the PFNT Pdot. More importantly, PFNT Pdot presents excellent photostability compared

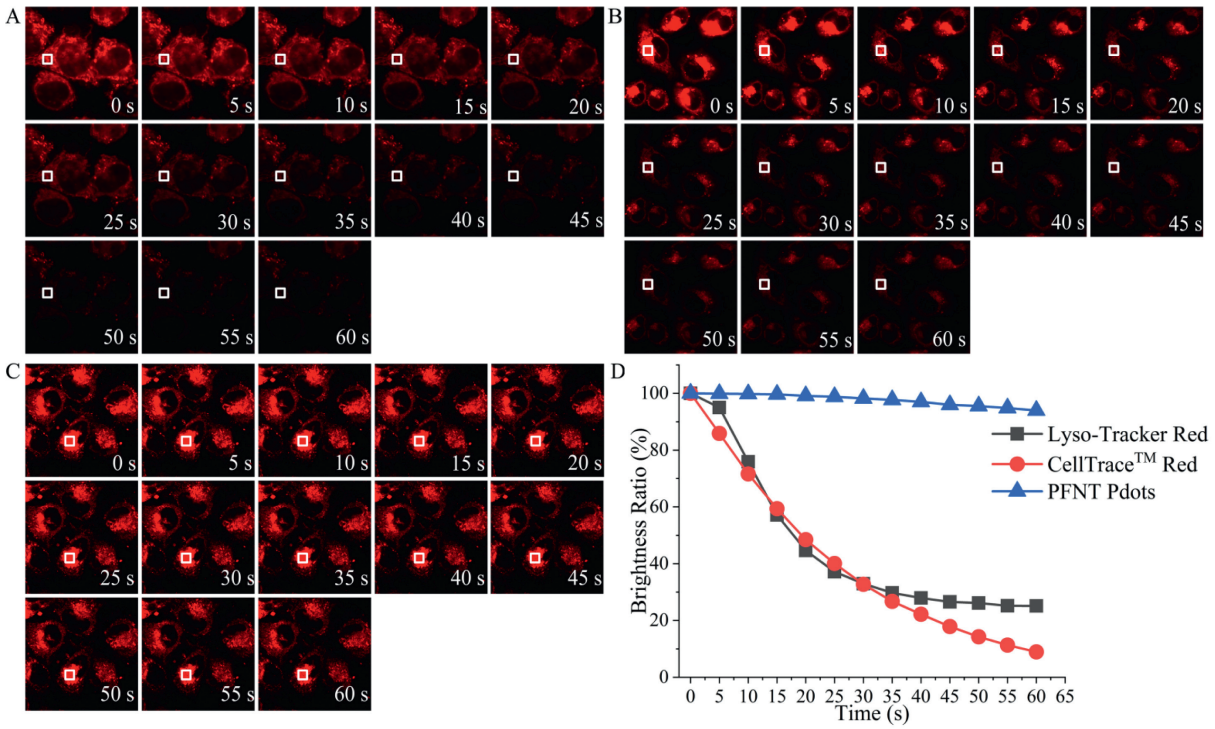

Fig. 3. Dynamic fluorescence images of time-sequential scanning by CLSM of HUVEC cells incubated with Lyso-Tracker Red (A), CellTrace™ Red CMTPX (B), and PFNT Pdot (C). λ_{ex}: 561 nm. Brightness ratio variations of the rectangle area at different time points (D).

to reference red dyes. This property is beneficial for long-time observation of cell activities, including proliferation and apoptosis, which could be utilized for potential applications such as neurosciences and pharmacy.

Declaration of competing interest

The authors declare that they have no known competing financial interests or personal relationships that could have appeared to influence the work reported in this paper.

Acknowledgments

We gratefully thank the support of the Hundred Talents Program of Sun Yat-sen University (No. 76190-18841211), Hebei DHRSS Research Fund, China (No. E2019100005), and the High-level Talents Research Star-up Project of Hebei University (No. 521000981336).

Supplementary materials

Supplementary material associated with this article can be found, in the online version, at doi:10.1016/j.cclet.2022.107867.

References

[1] J. Li, R. Jiang, Q. Wang, et al., Biomaterials 217 (2019) 119304.
[2] C. Xie, W. Zhou, Z. Zeng, et al., Chem. Sci 11 (2020) 10553–10570.
[3] Y. Cai, Z. Wei, C. Song, et al., Chem. Soc. Rev. 48 (2019) 22–37.
[4] Y.Duan Kenry, B. Liu, Adv. Mater. 30 (2018) 1802394.
[5] X. Fu, H. Bai, F. Lyu, et al., Chem. Res. Chin. U. 36 (2020) 237–242.
[6] C. Wu, D.T. Chiu, Angew. Chem. Int. Ed. 52 (2013) 3086–3109.
[7] J. Yu, C. Wu, Z. Tian, et al., Nano Lett. 12 (2012) 1300–1306.
[8] J. Li, K. Pu, Chem. Soc. Rev. 48 (2019) 38–71.
[9] Y. Yuan, W. Hou, W. Qin, et al., Biomater. Sci. 9 (2021) 328–346.
[10] N. Alifu, A. Zebibula, H. Zhang, et al., Nano Res. 13 (2020) 2632–2640.
[11] H. Chen, J. Yu, J. Zhang, et al., Angew. Chem. Int. Ed. 60 (2021) 19331–19336.
[12] Y. Tang, Z. Meng, H. Xu, et al., Chin. Chem. Lett. 28 (2017) 2164–2168.
[13] P. Yang, X. Zhou, J. Zhang, et al., Green Chem. 23 (2021) 1834–1839.
[14] Z. Li, T. Wang, F. Zhu, et al., Chin. Chem. Lett. 31 (2020) 783–786.
[15] C. Wu, B. Bull, C. Szymanski, et al., ACS Nano 2 (2008) 2415–2423.
[16] X. Zhang, J. Yu, C. Wu, et al., ACS Nano 6 (2012) 5429–5439.
[17] J. Sun, H. Mel, S. Wang, et al., Anal. Chem. 88 (2016) 7372–7377.
[18] L. Chen, D. Chen, Y. Jiang, et al., Angew. Chem. Int. Ed. 58 (2019) 7008–7012.
[19] J. Qi, C. Sun, D. Li, et al., ACS Nano 12 (2018) 7936–7945.
[20] Z. Zhang, X. Fang, Z. Liu, et al., Angew. Chem. Int. Ed. 59 (2020) 3691–3698.
[21] X. Cai, B. Liu, Angew. Chem. Int. Ed. 59 (2020) 9868–9886.
[22] S. Liu, H. Ou, Y. Li, et al., J. Am. Chem. Soc. 142 (2020) 15146–15156.
[23] H. Liu, P. Wu, S. Kuo, et al., J. Am. Chem. Soc. 137 (2015) 10420–10429.
[24] I.C. Wu, J. Yu, F. Ye, et al., J. Am. Chem. Soc. 137 (2015) 173–178.
[25] B. Andreiuk, A. Reisch, M. Lindecker, et al., Small 13 (2017) 1701582.
[26] C. Ke, C. Fang, J. Yan, et al., ACS Nano 11 (2017) 3166–3177.
[27] S. Wang, J. Liu, G. Feng, et al., Adv. Funct. Mater. 29 (2019) 1808365.
[28] S. Xu, Y. Duan, B. Liu, Adv. Mater. 32 (2020) 1903530.
[29] W. Tsai, C. Wang, C. Liao, et al., Chem. Sci. 10 (2019) 198–207.
[30] L. Chen, L. Wang, X. Jing, et al., J. Mater. Chem. 21 (2011) 10265–10267.
[31] W. Li, Y. Pan, L. Yao, et al., Adv. Opt. Mater. 2 (2014) 892–901.
[32] L. Chen, X. He, Y. Zhao, Mater. Adv. 2 (2021) 6068–6074.
[33] L. Chen, H. Tong, Z. Xie, et al., J. Mater. Chem. 21 (2011) 15773–15779.
[34] L. Chen, L. Wu, J. Yu, et al., Chem. Sci. 8 (2017) 7236–7245.
[35] L.P. Fernando, P.K. Kandel, J. Yu, et al., Biomacromolecules 11 (2010) 2675–2682.
[36] Y. Jin, F. Ye, C. Wu, et al., Chem. Commun. 48 (2012) 3161–3163.